Delay multiply and sum beamforming in 3D coherent multi-transducer ultrasound for contrast enhancement in the presence of acoustic clutter

Paul Dryburgh*, Daniele Mazierli†, Joseph V Hajnal*, Piero Tortoli‡, Alessandro Ramalli†, and Laura Peralta*
*School of Biomedical Engineering & Imaging Sciences, King's College London, London, UK
Email: paul.dryburgh@kcl.ac.uk; jo.hajnal@kcl.ac.uk; laura.peralta_pereira@kcl.ac.uk
†Department of Information Engineering, University of Florence, Florence, Italy
Email: daniele.mazierli@unifi.it; alessandro.ramalli@unifi.it; piero.tortoli@unifi.it

***Abstract*—Transducers with larger aperture size are desirable in ultrasound imaging to improve resolution and image quality. However, in practice inhomogeneities and aberrating layers cause phase errors that limit the benefits of increased aperture size. A coherent multi-transducer ultrasound (CoMTUS) imaging system enables an extended effective aperture through coherent combination of multiple transducers. In this work, an implementation of the Filtered Delay Multiply and Sum (F-DMAS) beamforming algorithm adapted to the specific aperture of CoMTUS imaging, was applied to 3D experimental data acquired in the presence of acoustic clutter and aberration. Results show F-DMAS applied to CoMTUS data suppresses the acoustic clutter across the image, with an increased dynamic range and improved detection of point targets. When further combined with the optimal beamforming parameters of CoMTUS, the impact of phase aberration effects along with the acoustic clutter is further reduced.**

***Index Terms*—CoMTUS, aberration, F-DMAS, sparse array, 3-D, plane wave, multi-array, ULA-OP**

I. Introduction

The quality of ultrasound images is limited by the spatial resolution and restricted field of view (FoV), particularly in applications requiring large penetration depths, including transabdominal and fetal imaging.

Despite a large aperture being desirable, the practical aperture size is often limited by the complexity and cost of scanners and arrays due to the number of channels required, and the low flexibility for some applications. To address this challenge, we have developed coherent multitransducer ultrasound (CoMTUS) imaging [1], which coherently combines the radio frequency (RF) data received by multiple synchronized arrays that take turns transmitting plane waves (PWs) into a common FoV, whilst backscattered echoes are received across all arrays. CoMTUS has been shown to offer an extended FoV, along with improved resolution and sensitivity in both 2D and 3D imaging [1], [2]. In the CoMTUS method, the optimal beamforming parameters, which include the transducers' location and the average speed of sound (SoS), are deduced by maximizing the coherence of the received echoes resulting from different targeted scatterers in the medium by cross-correlation.

However, the enlarged but discontinuous effective aperture presents additional challenges for the current Delay and Sum (DAS) beamforming algorithm, which may degrade contrast. Additionally, the actual improvements offered by the extended effective aperture can be further limited when moving to in vivo ultrasound due to presence of wavefront aberrations and acoustic clutter [3]. Typically, US images are reconstructed using a single SoS, and the mismatch between the assumed and actual SoS distribution limits US image resolution and contrast [4]. This is particularly true in transabdominal imaging of patients with large body habitus [5]. Furthermore, there is the challenge of reverberation, due to multiple reflections generating clutter that distorts the appearance of the wavefronts from the region of interest.

The filtered delay multiply and sum (F-DMAS) beamforming algorithm has been shown to improve ultrasound image quality by suppressing noise, enhancing contrast resolution, and increasing dynamic range [6], [7]. In the presence of acoustic clutter it is hypothesized artifacts will be suppressed through F-DMAS compared to DAS. Furthermore, as the average SoS is part of the optimization process in the CoMTUS method, some aberration correction is expected.

This study aims to advance the use of CoMTUS for future 3D in vivo applications by investigating its performance in the presence of phase aberration and acoustic clutter using sparse matrix arrays [8]. Specifically, we focus on applying F-DMAS beamforming to CoMTUS data and optimizing the SoS estimation to mitigate the effects of aberrating layers on beamformed images."

II. Methods

A. Experimental setup

The experimental setup is outlined in Fig. 1. The experimental data were acquired by using two synchronized ULA-OP 256 systems in a master-client configuration (MSD Laboratory, University of Florence, Florence, Italy) [9] with a pair of 2-D sparse spiral arrays (Vermon S.A., Tours, France), whose

This research was funded by the Royal Society (URF/R1/211049). The Department of Information Engineering, University of Florence, was supported by the Italian Ministry of Education, University and Research (PRIN 2020) under grant number 20205HFXE7

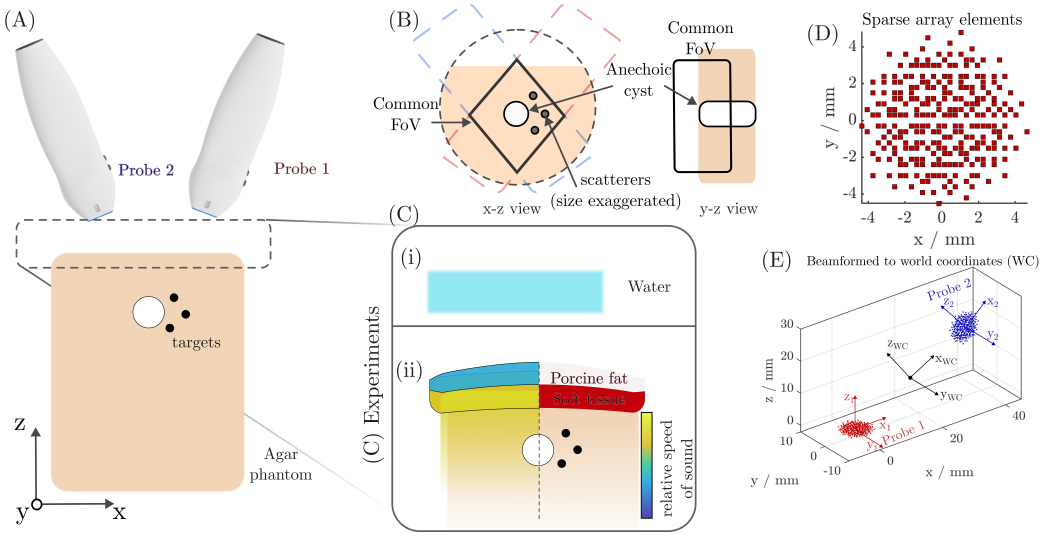

Fig. 1. Experimental layout and hardware configuration used. (A) Arrangement of arrays relative to agar phantom, showing cyst region and point-like spherical targets. The dashed region indicates where the aberrating layer is introduced. (B) The FoV of the two arrays, and the common FoV in the x-z and y-z planes. (C) Layers between arrays and phantom for the two acquisitions (i) water, and (ii) porcine layer. (D) The position of the 256 elements, in local coordinates, of the sparse array. (E) The elements of both arrays indicating relative positions between the arrays and the global coordinate system used for beamforming aligning the origin with the centre of the created effective aperture.

design was described in [10]. As shown in Fig. 1(a), the two arrays were positioned, using a 3D printed holder, to scan a common volume of interest including a purposely developed phantom, which consisted of three point targets and an anechoic cylindrical inclusion of 6.5 mm diameter in a homogeneous agar-agar background. Fig. 1(b) outlines the FoV of both arrays and the beamformed planes presented in this work. A transmit/receive sequence in which one of the arrays transmits PWs while both arrays receive was implemented in the ULA-OP 256 systems. A sequence of 9 PWs was transmitted by each array, i.e., with steering angles in a range of 5º with a step size of 2.5º in both the lateral (x-axis) and elevational (y-axis) directions. No apodisation was applied on transmission or reception.

The array holder was selected to have the FoV intersect at a depth of $40\,\mathrm{mm}$, and to place the arrays as close together as practical, in order to minimize the side-lobe artifacts generated from the discontinuous aperture [11]. The position of array 2, relative to array 1, can be described by the translations $\mathbf{T}$ and rotations $\mathbf{R}$ required to position array 2. The designed values in this work were $\mathbf{T} = [34, 0, 14.4]\mathrm{mm}$, and $\mathbf{R} = [0°, -50°, 0°]$. This creates an extended aperture in the x-axis, therefore the benefits of CoMTUS are expected in this direction.

Two sets of acquisitions were completed, as outlined in Fig. 1(c). As a control case (i), acquisitions were taken with no layer between the arrays and the agar phantom. Secondly (ii), acquisitions were then made with a porcine layer, of $\sim 25\,\mathrm{mm}$ thickness, on top of the agar phantom to induce phase aberration and reverberation effects. Raw data were acquired on the 256 elements of the array, Fig. 1(d) and CoMTUS images were beamformed off-line. The CoMTUS optimal beamforming parameters were found by maximizing

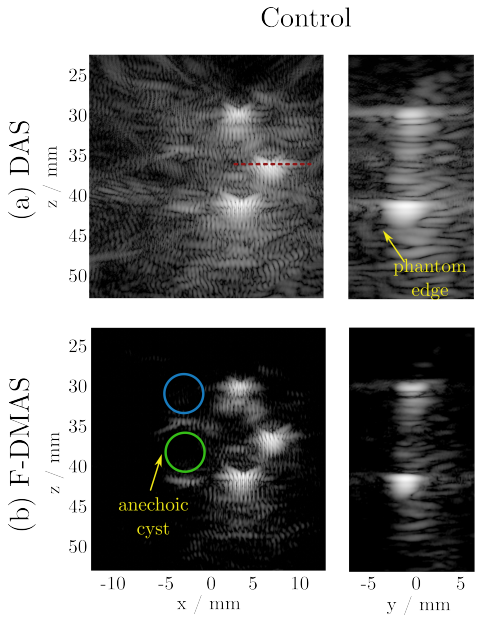

Fig. 2. CoMTUS B-mode images from control acquisition beamformed with DAS (a) and F-DMAS (b). Images present (left) $x - z$ and (right) $y - z$ planes. Blue and green regions indicate the signal and anechoic regions used for contrast assessment, respectively. Red dashed line indicates position of lateral profile in Fig.4. Dynamic range 50 dB.

the spatial coherence across the effective aperture from the three point targets [2]. The calibration was conducted from the data obtained from the control case, and then calculated for the porcine data to allow the SoS to vary. Acquired RF datasets were band-pass (BP) filtered, either to the bandwidth of the array for DAS, or twice the central frequency for F-DMAS. Beamformed images were envelop detected, log-compressed

and normalized to give the final CoMTUS B-mode images. CoMTUS images beamformed by DAS were compared with those obtained by the specific F-DMAS for CoMTUS [12].

III. Results

Fig. 2 shows the CoMTUS B-mode image beamformed with DAS for the control case. The image is beamformed using the optimal beamforming parameters $\mathbf{T} = [34.1, -0.5, 19.9]\,\mathrm{mm}$ and $\mathbf{R}$ parameterized by the angles $[-1.5°, -50.3°, -3.4°]$ with a SoS found to be $1496\,\mathrm{ms}^{-1}$. The point targets are correctly beamformed, and the edge of the phantom is well defined.

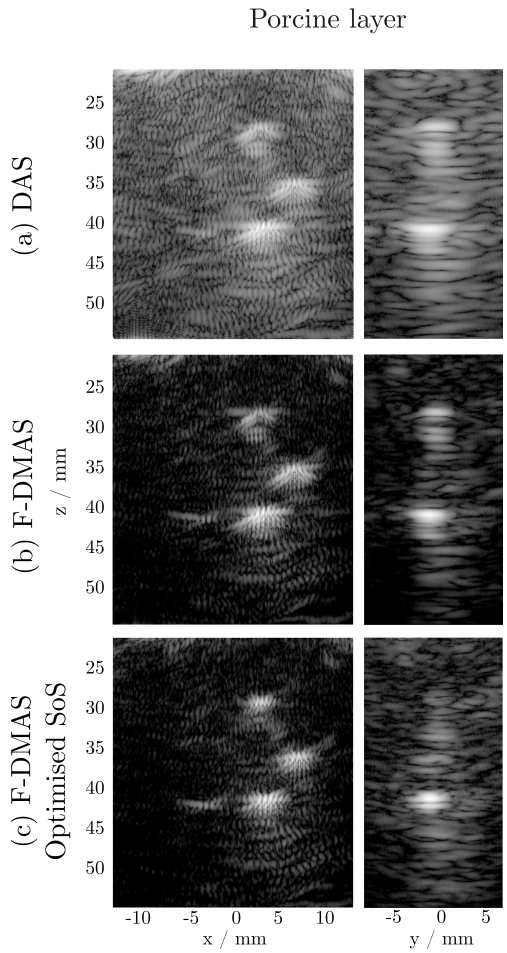

Fig. 3. CoMTUS B-mode images from porcine layer experiment. x-z planes shown in left-hand column, y-z plane in right-hand. Dynamic range 60 dB

Fig. 3 presents the results from the porcine layer experiment, where both reverberation and phase aberration artifacts would be expected. In the DAS image (a), significant acoustic clutter is observed and the cystic region cannot be discerned. Observation of the point targets clearly shows the datasets have not been coherently combined successfully. From Fig. 3(b), applying F-DMAS beamforming to this dataset successfully suppresses a significant amount of acoustic clutter, enhancing the visibility of the target and cyst wall. However, the targets remain poorly beamformed, due to the phase aberration. In Fig. 3(c) the SoS was re-calibrated, following the CoMTUS optimization procedure, allowing for the change in average SoS from the introduction of the porcine layer. The resulting image is qualitatively similar to the control image with no aberating layer, indicating the effects of phase aberration and clutter have been minimized.

TABLE I
Measured contrast metrics.

	Control		Porcine layer	
	DAS	F-DMAS	DAS	F-DMAS
CR [dB]	-13.7	-17.9	-3.6	-4.2047
CNR [-]	1.12	0.72	0.4551	0.5212
gCNR [-]	0.74	0.53	0.2846	0.3267

Table I compares the contrast metrics for DAS and F-DMAS beamforming for the control and porcine layer experiments. For the control case, F-DMAS outperforms DAS in terms of CR, as would be expected. Whereas a lower CNR (0.72 vs 1.12) and gCNR (0.53 vs 0.74) was observed for the F-DMAS, due to the increased speckle variance [13]. For the phase aberration phantom, the F-DMAS method with optimised SoS, shows improvement compared to DAS across the three metrics.

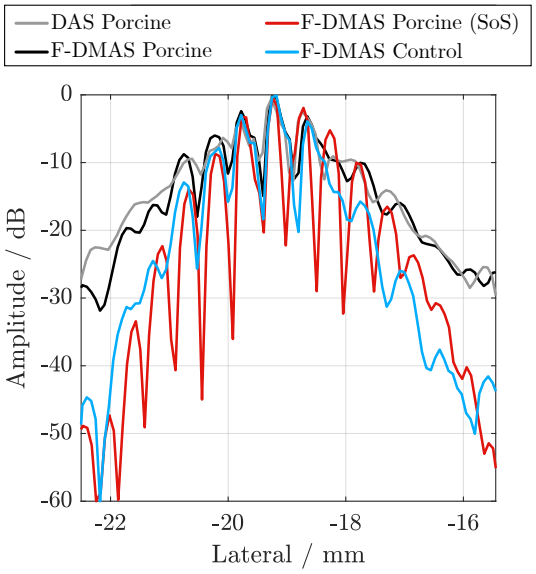

Fig. 4. Lateral profiles through middle point target in x-z plane from porcine phantom for (grey) DAS, (black) F-DMAS and (red) F-DMAS combined with optimised SoS. The result from the same target in the control phantom, beamformed with F-DMAS, is also shown (blue).

Finally, Fig. 4 plots the lateral profile through the middle target (see red dashed line in Fig.2(a)) for the three beamforming approaches applied to the porcine phantom, along with the F-DMAS result from the control phantom, for baseline comparison. The lateral profiles highlight the combination of F-DMAS and SoS calibration return to a result similar to the

control image, in terms of formation of the point target.

Whilst the F-DMAS algorithm necessitates a higher number of more complex operations, $(N^2 - N)/2$ compared to N for DAS, a real-time implementation of F-DMAS has been already demonstrated [14]. Future studies will focus on a real time implementation of F-DMAS for CoMTUS and an in vivo demonstration [15].

IV. Conclusions

In this work, the combination of F-DMAS beamformer with CoMTUS was shown to be robust to acoustic clutter, significantly suppressing artifacts. The SoS calibration was then able to compensate for the effects of phase aberration.

References

[1] L. Peralta, A. Gomez, Y. Luan, B. H. Kim, J. V. Hajnal, and R. J. Eckersley, "Coherent multi-transducer ultrasound imaging," *IEEE Transactions on Ultrasonics, Ferroelectrics, and Frequency Control*, vol. 66, no. 8, pp. 1316–1330, aug 2019.

[2] L. Peralta, D. Mazierli, A. Gomez, J. V. Hajnal, P. Tortoli, and A. Ramalli, "3-D Coherent Multitransducer Ultrasound Imaging With Sparse Spiral Arrays," *IEEE Transactions on Ultrasonics, Ferroelectrics, and Frequency Control*, vol. 70, no. 3, pp. 197–206, 2023.

[3] V. H. van Hal, J. W. Muller, M. R. van Sambeek, R. G. Lopata, and H. M. Schwab, "An aberration correction approach for single and dual aperture ultrasound imaging of the abdomen," *Ultrasonics*, vol. 131, no. February, 2023.

[4] Y. Li, "Correction of phase aberrations in medical ultrasound images using signal redundancy," *Ultrasound Imaging-Medical Applications*, 2011.

[5] L. M. Hinkelman, T. D. Mast, L. A. Metlay, and R. C. Waag, "The effect of abdominal wall morphology on ultrasonic pulse distortion. Part I. Measurements," *The Journal of the Acoustical Society of America*, vol. 104, no. 6, pp. 3635–3649, 1998.

[6] G. Matrone, A. S. Savoia, G. Caliano, and G. Magenes, "The delay multiply and sum beamforming algorithm in ultrasound B-mode medical imaging," *IEEE Transactions on Medical Imaging*, vol. 34, no. 4, pp. 940–949, 2015.

[7] G. Matrone, A. S. Savoia, C. Giosue, and G. Magenes, "Ultrasound plane-wave imaging with delay multiply and sum beamforming and coherent compounding," in *2016 38th Annual International Conference of the IEEE Engineering in Medicine and Biology Society (EMBC)*, 2016, pp. 3223–3226.

[8] A. Ramalli, E. Boni, E. Roux, H. Liebgott, and P. Tortoli, "Design, Implementation, and Medical Applications of 2-D Ultrasound Sparse Arrays," *IEEE Transactions on Ultrasonics, Ferroelectrics, and Frequency Control*, vol. 69, no. 10, pp. 2739–2755, 2022.

[9] D. Mazierli, A. Ramalli, E. Boni, F. Guidi, and Tortoli, "Architecture for an Ultrasound Advanced Open Platform with an Arbitrary Number of Independent Channels," *IEEE Transactions on Biomedical Circuits and Systems*, vol. 15, no. 3, pp. 486–496, 2021.

[10] A. Ramalli, S. Harput, S. Bézy, E. Boni, R. J. Eckersley, P. Tortoli, and J. D'hooge, "High-frame-rate tri-plane echocardiography with spiral arrays: From simulation to real-time implementation," *IEEE Transactions on Ultrasonics, Ferroelectrics, and Frequency Control*, vol. 67, no. 1, pp. 57–69, 2019.

[11] L. Peralta, D. Mazierli, K. Christensen-Jeffries, A. Ramalli, P. Tortoli, and J. V. Hajnal, "On the Arrays Distribution, Scan Sequence and Apodization in Coherent Dual-Array Ultrasound Imaging Systems," *Applied Sciences (Switzerland)*, vol. 13, no. 19, p. 10924, oct 2023.

[12] L. Peralta, D. Mazierli, J. V. Hajnal, P. Tortoli, and A. Ramalli, "Specific Delay Multiply and Sum Beamforming for 2-D and 3-D Coherent Multi-Transducer Ultrasound imaging," in *2022 IEEE International Ultrasonics Symposium (IUS)*, 2022, pp. 1–3.

[13] F. Prieur, O. M. H. Rindal, and A. Austeng, "Signal coherence and image amplitude with the filtered delay multiply and sum beamformer," in *IEEE Transactions on Ultrasonics, Ferroelectrics, and Frequency Control*, vol. 65, no. 7. Institute of Electrical and Electronics Engineers Inc., jul 2018, pp. 1133–1140.

[14] A. Ramalli, M. Scaringella, G. Matrone, A. Dallai, E. Boni, A. S. Savoia, L. Bassi, G. E. Hine, and P. Tortoli, "High dynamic range ultrasound imaging with real-time filtered-delay multiply and sum beamforming," in *2017 IEEE International Ultrasonics Symposium (IUS)*, 2017, pp. 1–4.

[15] D. Mazierli, A. Ramalli, A. Dallai, E. Skelton, J. V. Hajnal, P. Tortoli, and L. Peralta, "Real-Time 2-D Coherent Multi-Transducer Ultrasound Imaging in Vivo," *IEEE International Ultrasonics Symposium, IUS*, pp. 1–4, 2023.